Preprint typeset in JHEP style. - HYPER VERSION

hep-ph/0109079
SLAC–PUB–8974
UCLA/01/TEP/18
September, 2001

QCD and QED Corrections to Light-by-Light Scattering

Z. Bern,* **A. De Freitas***

Department of Physics and Astronomy
UCLA, Los Angeles, CA 90095-1547

L. Dixon†

Stanford Linear Accelerator Center
Stanford University
Stanford, CA 94309

A. Ghinculov* **and H.L. Wong***

Department of Physics and Astronomy
UCLA, Los Angeles, CA 90095-1547

Abstract: We present the QCD and QED corrections to the fermion-loop contributions to light-by-light scattering, $\gamma\gamma \to \gamma\gamma$, in the ultrarelativistic limit where the kinematic invariants are much larger than the masses of the charged fermions.

Keywords: two-loop; QED; quantum electrodynamics; photon-photon.

Submitted to JHEP

*Research supported by the US Department of Energy under grant DE-FG03-91ER40662.
†Research supported by the US Department of Energy under grant DE-AC03-76SF00515.

1. Introduction

Light-by-light scattering is one of the most fundamental processes in QED. Theoretically, it proceeds at leading order, $\mathcal{O}(\alpha^4)$, via one-loop box diagrams containing charged particles. At center-of-mass energies $\sqrt{s}$ far below the mass of the electron, the process is described by the Euler-Heisenberg effective Lagrangian [1], and the cross section rises rapidly with energy, $\sigma \propto s^3/m_e^8$. The cross section peaks at $\sqrt{s} \approx 3m_e$ [2], then begins to fall rapidly, $\sigma \propto 1/s$ at fixed angles for $s \gg m_e^2$ [3]. At still higher energies, similar thresholds are crossed for the muon, tau, and light quarks – or rather, the light hadrons. (See fig. 1.) The final significant Standard Model thresholds reached are those of the W boson [4, 5] and the top quark.

The direct experimental evidence for $\gamma\gamma \to \gamma\gamma$ scattering is still scant, particularly for energies above a few GeV. At optical (electron volt) energies, at least two experiments have been proposed to detect the Euler-Heisenberg interaction via birefringence of the vacuum using laser photons in a magnetic field [6]. The Crystal Ball experiment at the SPEAR storage ring had some unpublished evidence for $\gamma\gamma \to \gamma\gamma$ scattering at $\sqrt{s}$ of order several MeV, after subtracting beam-off γ ray backgrounds [7]. More extensive data are available for the process of Delbrück scattering, in which two of the four photons are supplied by the Coulomb field of a nucleus. Several experiments have studied this process, for incident photon energies ranging from a few MeV to about a GeV. Higher order Coulomb ($Z\alpha$) corrections are often important in the comparison with theory [8]. Light-by-light scattering via an electron loop is also tested quite precisely, if indirectly, by the measurement of the anomalous magnetic moment of the electron [9], as well as that of the muon [10] (the latter is even sensitive to muonic and hadronic light-by-light scattering).

At much higher energies, the small size of the Standard Model light-by-light scattering cross section provides a potential window to new physics. By backscattering a laser pulse off an intense, high energy electron beam [11], it is possible to create $\gamma\gamma$ collisions with $\sqrt{s}$ of order 100–1000 GeV, high levels of initial state polarization, and luminosities of order tens of fb^{-1} per year. It has been shown that the $\gamma\gamma \to \gamma\gamma$ process at high energies is a sensitive probe [12] of theories with large extra dimensions [13], for example. Despite this interest in light-by-light scattering, the process has to date only been calculated to leading order (one loop), except in the low energy limit, where the two-loop corrections to the Euler-Heisenberg Lagrangian are known [14].

In this paper, we present the two-loop corrections to $\gamma\gamma \to \gamma\gamma$ in the ultra-relativistic regime where the kinematic invariants s, t, u are much greater than the (squared) charged fermion masses. This regime is relevant for two ranges of center of mass energy in the Standard Model:

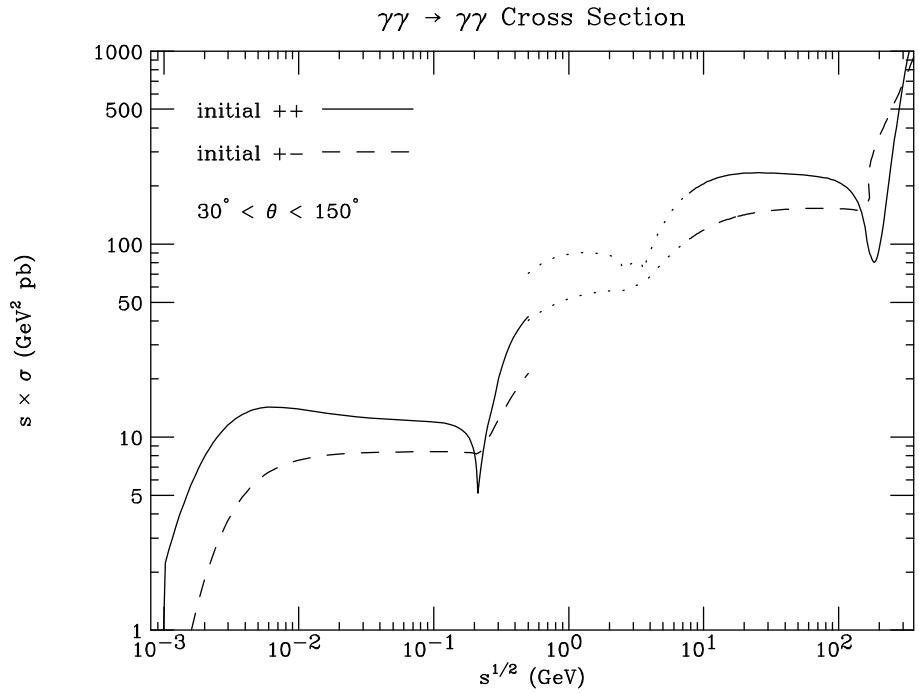

Figure 1: The leading order (one loop) cross section for light-by-light scattering, for intermediate energies, showing the light fermion thresholds. The cross section has been integrated over a range of center-of-mass scattering angles, $30^\circ < \theta < 150^\circ$, for the two independent choices of initial photon helicities (assuming CP invariance), $++$ (solid) and $+-$ (dashed). We have multiplied σ by s merely to compress the dynamic range. We set $\alpha = 1/137.036$. For $\sqrt{s} < 0.5$ GeV we omit all quark loops but include the charged pion and kaon loops. For $\sqrt{s} > 0.5$ GeV we use the quark loops, with $m_u = m_d = 5$ MeV, $m_s = 100$ MeV, $m_c = 1.25$ GeV, $m_b = 4.2$ GeV, $m_t = 175$ GeV, and $m_W = 80.42$ GeV. The hadronic contribution to the region from 0.5 to 8 GeV is not computed reliably by the quark boxes; hence that region is shown dotted. We also omit the hadronic resonance contributions, π^0, η, etc.

- For $m_c \ll \sqrt{s} \lesssim 2m_W$ (and neglecting the tiny bottom quark contribution), the QCD corrections from attaching a gluon line to the quark box are most important. These give rise to finite $\mathcal{O}(\alpha^4\alpha_s)$ corrections to the cross section.

- For $m_e \ll \sqrt{s} \lesssim 2m_\mu \approx 2m_\pi$, the dominant corrections are QED corrections from attaching a photon line to the electron box. There are also QED corrections from inserting a fermion loop onto an external leg; however, these are cancelled completely if the theory is renormalized at zero momentum transfer, i.e. by using $\alpha \equiv \alpha(0) = 1/137.036\ldots$ as the coupling constant. Then the two-loop QED corrections become identical to those of QCD, up to an overall constant.

The Feynman diagrams for $\gamma\gamma \to \gamma\gamma$ at two loops are a small subset of those required for gluon-gluon scattering, $gg \to gg$. The interference of these two loop amplitudes with the $gg \to gg$ tree amplitudes is an essential ingredient for obtaining the next-to-next-to-leading order QCD corrections to jet production at hadron colliders. This interference was recently evaluated in a tour de force calculation by Glover, Oleari and Tejeda-Yeomans [15]. In the light-by-light case, the tree amplitudes vanish. Thus the *next*-to-leading order corrections require a different interference, of two-loop amplitudes with one-loop amplitudes. Instead of evaluating this interference directly, we have computed the two-loop $\gamma\gamma \to \gamma\gamma$ amplitudes in a helicity basis. Thus polarized as well as unpolarized cross sections can be obtained, information which is quite useful in the photon case, because of the high initial state photon polarizations that are possible with backscattering.

Rather than calculating the Feynman diagrams for the two-loop $\gamma\gamma \to \gamma\gamma$ helicity amplitudes, we employed a unitarity- or cut-based technique [16, 17, 18] to generate the required loop momentum integrals. These integrals were then evaluated using techniques recently developed [19, 20, 21] to handle double box and related integrals where all internal lines are massless. The restriction to massless internal lines limits the validity of our results to the ultrarelativistic region where all kinematic invariants are much greater than the relevant fermion masses.

Remarkably, some of the helicity amplitudes stay quite simple, even at two loops. Some of this simplicity can be understood via unitarity and supersymmetry Ward identities [22].

This paper is organized as follows. In section 2 we present analytic results for the two-loop $\gamma\gamma \to \gamma\gamma$ helicity amplitudes. (The more complicated formulae are relegated to an appendix.) In section 3 we give numerical results for the QCD and QED corrections. In section 4 we present our conclusions.

2. The Two-Loop Amplitudes

The one-loop Feynman diagrams for photon-photon scattering via a charged fermion consist of six box diagrams, which are related by permutations of the external photons to the diagram shown in fig. 2a. At two loops, there are $6 \cdot 10 = 60$ nonvanishing Feynman diagrams, corresponding to connecting any two sides of the box with a photon propagator (or a gluon propagator, in the case that the charged fermion is a quark). Up to permutations, these diagrams are depicted in fig. 2b. Diagrams consisting of two separate charged fermion triangles connected by a single photon or gluon, as illustrated in fig. 2c, vanish by Furry's theorem [23] or simple group theory.

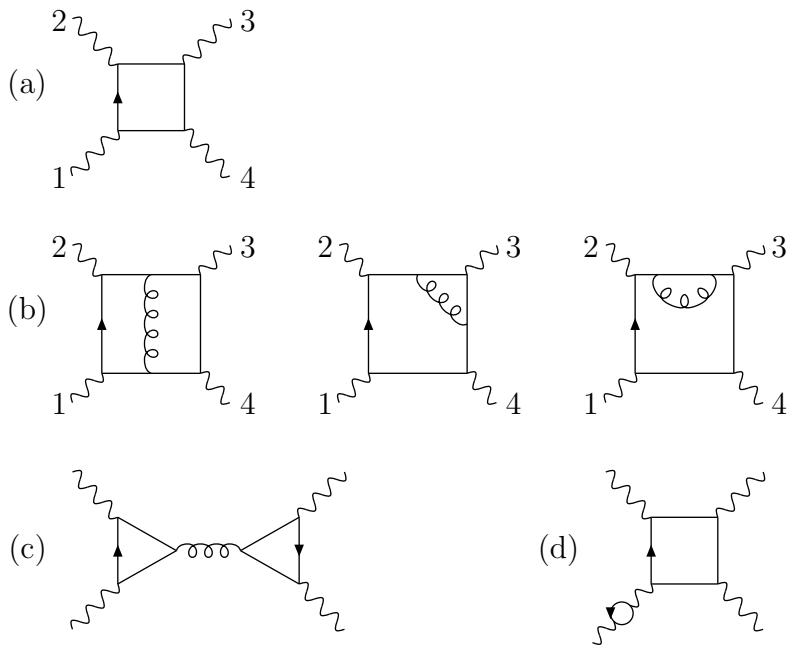

Figure 2: Feynman diagrams for light-by-light scattering via a charged fermion loop. (a) One of the six box diagrams contributing at one loop; the remaining diagrams are obtained by permuting the external photons. (b) The three types of diagrams contributing at two loops; the rest of the 60 diagrams are obtained by permutations. The curly line can be either a photon or a gluon, depending on whether the QED or QCD correction is being computed. (c) These diagrams vanish by Furry's theorem or simple group theory. (d) These diagrams could contribute to the QED correction. However, they are precisely cancelled by conventional on-shell renormalization.

We did not evaluate the Feynman diagrams directly. Instead we computed the unitarity cuts in various channels, working to all orders in the dimensional regularization parameter $\epsilon = (4 - D)/2$. Essentially we followed the approach first employed at two loops for the special cases of $N = 4$ supersymmetric amplitudes [17] and the pure gluon four-point amplitude with all plus helicities [18]. These amplitudes were simple enough that a compact expression for the integrand could be given. The fermion loop contributions with all plus helicities are about as simple [24]. However, for the generic helicity configuration, the integrands become quite complicated.

We have used general integral reduction algorithms developed for the all-massless planar four-point topologies [19, 20], in order to reduce the loop integrals to a minimal basis of master integrals. Some mild extensions of these techniques are required in order to incorporate polarization vectors for photons of definite helicity [25]. We then expand the master integrals in a Laurent series in ϵ, which begins at order $1/\epsilon^4$. Many of

the master integral Laurent expansions quoted in refs. [19, 20] are in terms of Nielsen functions [26], usually denoted by $S_{n,p}(x)$, with $n+p \leq 4$. However, using various identities [27] the results can be expressed in terms of the polylogarithms [28],

$$\begin{aligned} \mathrm{Li}_n(x) &= \sum_{i=1}^{\infty} \frac{x^i}{i^n} = \int_0^x \frac{dt}{t} \mathrm{Li}_{n-1}(t), \\ \mathrm{Li}_2(x) &= -\int_0^x \frac{dt}{t} \ln(1-t)\,, \end{aligned} \tag{2.1}$$

with $n = 2, 3, 4$.

It is reassuring that all of the poles in ϵ cancel for each helicity amplitude in the QCD case. In QCD, two loops is the first order at which α_s appears in the $\gamma\gamma \to \gamma\gamma$ amplitude; therefore there can be no ultraviolet divergence. Any infrared divergence would have to be cancelled by real gluon radiation; but the process $\gamma\gamma \to \gamma\gamma g$ is forbidden by group theory.

In addition to infrared finiteness, the calculational framework was also tested by gauge invariance: replacing a photon polarization vector by its momentum vector produces a vanishing result. Finally, the same computer programs for evaluating the cuts and reducing the integrals were also used to compute the fermion-loop contribution to the two-loop $gg \to gg$ amplitudes in the helicity formalism and the 't Hooft-Veltman dimensional regularization scheme [25]. The interference of the two-loop $gg \to gg$ helicity amplitudes with the tree amplitudes, after summing over all external helicities and colors and accounting for the different scheme used, is in complete agreement with the calculation using conventional dimensional regularization [15].

The QED case requires exactly the same set of two-loop diagrams as in QCD, up to an overall factor. In addition, there are external fermion bubble insertions of the form shown in fig. 2d. In dimensional regularization with massless fermions, these diagrams would vanish by virtue of containing scale-free integrals. This vanishing represents a cancellation of ultraviolet and infrared divergences. However, if one renormalizes QED in the conventional on-shell scheme, to avoid infrared divergences one should retain a fermion mass in the external bubbles. Now the bubble integral is nonzero and ultraviolet-divergent. But this divergence, and indeed the entire integral, is exactly cancelled by the on-shell-scheme counterterm, precisely because the external leg is a real, on-shell photon.

Hence the on-shell-renormalized two-loop QED-corrected amplitude is the same as the two-loop QCD-corrected amplitude, up to overall coupling constant factors. In the on-shell scheme, the coupling constant should of course be set to $\alpha \equiv \alpha(0) = 1/137.036\ldots$. This value should be used for all the QED couplings associated with the real, external photons — that is, for all couplings *except* the extra one associated

with the virtual photon in each two-loop graph. The typical virtuality of the extra photon is not zero, but of order s, assuming that the kinematic invariants s, t, u are all comparable in magnitude and much larger than the squared fermion mass, m_f^2. Thus a running coupling $\alpha(\mu)$ with $\mu \approx \sqrt{s}$ should be used for the virtual photon insertion; whether it should be the $\overline{\rm MS}$ running coupling, or that defined via the photon propagator at momentum transfer μ, is theoretically indistinguishable at this order. For $m_e \ll \mu < m_\mu$, the latter coupling at one-loop order is

$$\alpha(\mu) \;=\; \frac{\alpha}{1 - \frac{\alpha}{3\pi}\left[\ln\left(\frac{\mu^2}{m_e^2}\right) - \frac{5}{3}\right]}\,. \tag{2.2}$$

For $\mu \gtrsim 2m_\pi$, the running of $\alpha(\mu)$ receives hadronic corrections as well, which are best evaluated via a dispersion relation using the $e^+e^- \to$ hadrons data. In any event, the precise $\alpha(\mu)$ used makes very little difference, since it only appears in an $\mathcal{O}(\alpha)$ correction to a process with a rather tiny cross section.

For the QCD corrections, we use the $\overline{\rm MS}$ running coupling $\alpha_s(\mu)$, again with $\mu = \sqrt{s}$, keeping in mind that our calculation is only to leading order in α_s.

We consider the process

$$\gamma(k_1,\lambda_1) + \gamma(k_2,\lambda_2) \;\to\; \gamma(k_3,\lambda_3) + \gamma(k_4,\lambda_4), \tag{2.3}$$

where k_i and λ_i are the photon momenta and helicities. In terms of the center-of-mass energy $\sqrt{s}$ and scattering angle θ, the Mandelstam variables are $s = (k_1+k_2)^2$, $t = (k_1-k_4)^2 = -s/2\times(1-\cos\theta)$, and $u = (k_1-k_3)^2 = -s/2\times(1+\cos\theta)$, with $s > 0$, $t < 0$, $u < 0$. Parity, time-reversal invariance, and Bose symmetry imply that there are only four independent helicity amplitudes, M_{--++}, M_{-+++}, M_{++++}, and M_{+--+}. Actually, crossing symmetry relates M_{++++} and M_{+--+}. However, representing the two-loop amplitudes in a crossing-symmetric fashion in terms of master integrals would lead to more cumbersome formulae, so we shall present all four amplitudes instead. We adopt the overall phase convention of refs. [4, 29]. Then formula (9) in ref. [29] can be applied to our helicity amplitudes in order to obtain the $\gamma\gamma \to \gamma\gamma$ differential cross section for generic circular and transverse photon polarizations (Stokes parameters).

The one-loop helicity amplitudes due to a fermion of mass m_f in the loop take a very simple form in the ultra-relativistic limit, $\{s,t,u\} \gg m_f^2$ [3, 2, 30]. We write

$$\mathcal{M}^{\text{1-loop}}_{\lambda_1\lambda_2\lambda_3\lambda_4} = 8\,NQ^4\,\alpha^2\,M^{(1)}_{\lambda_1\lambda_2\lambda_3\lambda_4}\,, \tag{2.4}$$

where N is the fermion color factor (3 for quarks, 1 for leptons), and Q is the fermion charge in units of e. The functions $M^{(1)}_{\lambda_1\lambda_2\lambda_3\lambda_4}$ are given by

$$M^{(1)}_{--++} = 1\,,$$

$$
\begin{aligned}
M^{(1)}_{-+++} &= 1, \\
M^{(1)}_{++++} &= -\frac{1}{2}\frac{t^2+u^2}{s^2}\Big[\ln^2\Big(\frac{t}{u}\Big)+\pi^2\Big] - \frac{t-u}{s}\ln\Big(\frac{t}{u}\Big) - 1\,, \\
M^{(1)}_{+--+} &= -\frac{1}{2}\frac{t^2+s^2}{u^2}\ln^2\Big(-\frac{t}{s}\Big) - \frac{t-s}{u}\ln\Big(-\frac{t}{s}\Big) - 1 \\
&\qquad - i\pi\Big[\frac{t^2+s^2}{u^2}\ln\Big(-\frac{t}{s}\Big) + \frac{t-s}{u}\Big]\,.
\end{aligned}
\tag{2.5}
$$

The QCD- and QED-corrected two-loop amplitudes are

$$
\begin{aligned}
\mathcal{M}^{\text{2–loop, QCD}}_{\lambda_1\lambda_2\lambda_3\lambda_4} &= 4\,(N^2-1)Q^4\,\alpha^2\,\frac{\alpha_s(\mu)}{\pi}\,M^{(2)}_{\lambda_1\lambda_2\lambda_3\lambda_4}\,, \\
\mathcal{M}^{\text{2–loop, QED}}_{\lambda_1\lambda_2\lambda_3\lambda_4} &= 8\,NQ^6\,\alpha^2\,\frac{\alpha(\mu)}{\pi}\,M^{(2)}_{\lambda_1\lambda_2\lambda_3\lambda_4}\,,
\end{aligned}
\tag{2.6}
$$

where the explicit values of the $M^{(2)}_{\lambda_1\lambda_2\lambda_3\lambda_4}$ are given in Appendix A.

Note from eq. (A.1) that M_{--++} remains remarkably simple even at two loops — it is just a constant, independent of s, t and u! This simplicity is actually predictable. The lack of an imaginary part for $M^{(2)}_{--++}$ (as for $M^{(1)}_{--++}$ and $M^{(1)}_{-+++}$) can be deduced by considering the possible unitarity cuts of the amplitude. Let f be a massless fermion. Then a supersymmetry Ward Identity [22] shows that the tree-level amplitudes for $\gamma\gamma f\bar{f}$ and $\gamma\gamma\gamma f\bar{f}$ vanish if all the photons have the same helicity (when considered as outgoing particles). The same result is true if one (or more) photons are replaced by gluons with the same helicity. Assigning opposite (outgoing) helicities to intermediate particles on opposite sides of a cut, it is easy to see that all two- or three-particle cuts vanish for the all-outgoing-plus-helicity two-loop amplitude $M^{(2)}_{--++}$. This argument assumes that a $D = 4$ helicity assignment is valid for the intermediate particles, a condition which is justified for the processes considered here by the absence of infrared or ultraviolet divergences. Thus $M^{(2)}_{--++}$ must be a dimensionless rational function. Crossing symmetry implies that it is totally symmetric in s, t, u. Imposing at most single poles in s, t, u, and using $s + t + u = 0$, one finds that $M^{(2)}_{--++}$ must actually be a constant.

Equation (A.2) shows that $M^{(2)}_{-+++}$ is also fairly simple, containing only logarithms, and not Li_2, Li_3 or Li_4 functions. Its two-particle cuts in $D = 4$ are the product of two rational functions (just like the cuts of a one-loop amplitude), which may partially account for this simplicity; however, the three-particle cuts do not similarly simplify at a glance.

Interestingly, up to the overall normalization these amplitudes are identical to the subleading color contributions for the $gg \to \gamma\gamma$ amplitudes presented in ref. [31]. (In that paper all particles are taken to be outgoing, which corresponds to flipping

the helicity labels for particles 1 and 2.) These amplitudes are relevant for improved estimates of the di-photon background to production of a light (mass < 140 GeV) Higgs boson at the Large Hadron Collider [32].

It is instructive to quote the values of the helicity amplitudes in various limits. The values of the one-loop functions for 90° scattering ($t = -s/2$, $u = -s/2$) are

$$\begin{aligned}
&M^{(1)}_{--++}(90^\circ) = 1\,,\\
&M^{(1)}_{-+-+}(90^\circ) = 1\,,\\
&M^{(1)}_{++++}(90^\circ) \approx -3.46740\,,\\
&M^{(1)}_{+--+}(90^\circ) \approx -0.12169 + 0.46574\pi i\,,
\end{aligned} \tag{2.7}$$

while the two-loop functions are

$$\begin{aligned}
&M^{(2)}_{--++}(90^\circ) = -1.5,\\
&M^{(2)}_{-+-+}(90^\circ) \approx 0.17770 - 0.23287\pi i\,,\\
&M^{(2)}_{++++}(90^\circ) \approx 1.24077 + 1.00717\pi i\,,\\
&M^{(2)}_{+--+}(90^\circ) \approx 0.01445 + 0.36840\pi i\,.
\end{aligned} \tag{2.8}$$

Note that except for the first, the two-loop functions are smaller than their one-loop counterparts.

In the small-angle limit $|t| \ll s$, the values of the one-loop amplitudes, up to corrections suppressed by powers of t/s, are

$$\begin{aligned}
&M^{(1)}_{--++} \sim 1\,,\\
&M^{(1)}_{-+-+} \sim 1\,,\\
&M^{(1)}_{++++} \sim -\frac{1}{2}X^2 - X - \frac{\pi^2}{2} - 1\,,\\
&M^{(1)}_{+--+} \sim -\frac{1}{2}X^2 - X - 1 - i\pi(X+1)\,,\\
&M^{(1)}_{+-+-} \sim 0\,,
\end{aligned} \tag{2.9}$$

while the two-loop amplitudes are,

$$\begin{aligned}
&M^{(2)}_{--++} \sim -\frac{3}{2}\,,\\
&M^{(2)}_{-+-+} \sim \frac{1}{4}X^2 + \frac{1}{2}X + \frac{\pi^2}{8} - \frac{1}{4} + i\pi\Big(\frac{1}{4}X + \frac{1}{4}\Big)\,,\\
&M^{(2)}_{++++} \sim -\frac{1}{24}X^4 - \frac{1}{12}X^3 - \Big(\frac{\pi^2}{12} + \frac{1}{2}\Big)X^2 - \Big(\frac{5}{12}\pi^2 + \frac{1}{2}\Big)X + \frac{7}{360}\pi^4 - \zeta_3 - \frac{7}{12}\pi^2 - \frac{1}{4}
\end{aligned}$$

$$
\begin{aligned}
&\quad + i\pi\Big(\frac{1}{2}X^2 + \frac{1}{2}X + 2\zeta_3 + \frac{\pi^2}{6} - \frac{13}{4}\Big)\,, \\
M^{(2)}_{+--+} &\sim -\frac{1}{24}X^4 - \frac{1}{12}X^3 + \Big(\frac{\pi^2}{6} - \frac{1}{2}\Big)X^2 + \Big(\frac{5}{6}\pi^2 - \frac{1}{2}\Big)X + \frac{11}{180}\pi^4 - \zeta_3 + \frac{5}{12}\pi^2 - \frac{1}{4} \\
&\quad + i\pi\Big(-\frac{1}{6}X^3 - \frac{3}{4}X^2 - \frac{3}{2}X - 2\zeta_3 + \frac{11}{4}\Big)\,, \\
M^{(2)}_{+-+-} &\sim -\frac{1}{2}\,,
\end{aligned}
\tag{2.10}
$$

where $X \equiv -\ln(-s/t)$. Notice that the small-angle scattering amplitudes where both photons flip their helicity have no logarithmic enhancements at one- or two-loops; those with one helicity flip have no logs at one loop but a factor of X^2 at two loops; and those with no helicity flips pick up one factor of X^2 for each loop. For small angles these contributions are actually power suppressed compared to t-channel vector exchange diagrams which first appear at three loops [33].

Next we give the differential cross sections in terms of the above amplitudes. The leading-order $\gamma\gamma \to \gamma\gamma$ unpolarized differential cross section for a single fermion flavor is given by

$$
\frac{d\sigma^{\rm LO}}{d\cos\theta} = N^2 Q^8 \,\frac{\alpha^4}{2\pi\, s}\Big[|M^{(1)}_{--++}|^2 + 4\,|M^{(1)}_{-+++}|^2 + |M^{(1)}_{++++}|^2 + |M^{(1)}_{+--+}|^2 + |M^{(1)}_{+-+-}|^2\Big]\,,
\tag{2.11}
$$

where

$$
M^{(L)}_{+-+-}(s,t,u) = M^{(L)}_{+--+}(s,u,t)\,.
\tag{2.12}
$$

The QCD- and QED-corrected unpolarized differential cross sections for a single fermion flavor are given by

$$
\begin{aligned}
\frac{d\sigma^{\rm QCD}}{d\cos\theta} &= \frac{d\sigma^{\rm LO}}{d\cos\theta} + \frac{d\sigma^{\alpha_s}}{d\cos\theta}\,, \\
\frac{d\sigma^{\rm QED}}{d\cos\theta} &= \frac{d\sigma^{\rm LO}}{d\cos\theta} + \frac{d\sigma^{\alpha}}{d\cos\theta}\,,
\end{aligned}
\tag{2.13}
$$

where

$$
\begin{aligned}
\frac{d\sigma^{\alpha_s}}{d\cos\theta} &= N(N^2-1)Q^8\,\frac{\alpha^4\,\alpha_s(\mu)}{2\pi^2\, s} I^{(2,1)}\,, \\
\frac{d\sigma^{\alpha}}{d\cos\theta} &= N^2 Q^{10}\,\frac{\alpha^4\,\alpha(\mu)}{\pi^2\, s} I^{(2,1)}\,,
\end{aligned}
\tag{2.14}
$$

and

$$
\begin{aligned}
I^{(2,1)} \equiv {\rm Re}\Big[&M^{(2)}_{--++} M^{(1)\,*}_{--++} + 4\, M^{(2)}_{-+++} M^{(1)\,*}_{-+++} + M^{(2)}_{++++} M^{(1)\,*}_{++++} \\
&+ M^{(2)}_{+--+} M^{(1)\,*}_{+--+} + M^{(2)}_{+-+-} M^{(1)\,*}_{+-+-}\Big]\,.
\end{aligned}
\tag{2.15}
$$

The cross sections for circularly polarized photons can be constructed easily from eq. (2.14) by reweighting the products of M's. For arbitrary initial photon polarizations, linear as well as circular, eqs. (9)–(15) of ref. [29] can be used, after making the replacement (for the QCD case)

$$F_{\lambda_1\lambda_2\lambda_3\lambda_4} \to \mathcal{M}_{\lambda_1\lambda_2\lambda_3\lambda_4} = 8\,NQ^4\,\alpha^2\,M^{(1)}_{\lambda_1\lambda_2\lambda_3\lambda_4} + 4\,(N^2-1)Q^4\,\alpha^2\,\frac{\alpha_s(\mu)}{\pi}\,M^{(2)}_{\lambda_1\lambda_2\lambda_3\lambda_4}\,. \tag{2.16}$$

(Note that our definitions of t and u are reversed with respect to ref. [29].)

3. Numerical Results

The QCD K factor is conventionally defined as the ratio of next-to-leading to leading-order cross sections,

$$K \equiv \frac{d\sigma^{\rm QCD}/d\cos\theta}{d\sigma^{\rm LO}/d\cos\theta}\,. \tag{3.1}$$

In a region between quark thresholds, and below the W mass, we can write

$$K = 1 + \frac{\alpha_s(\mu)}{\pi}\,\frac{\sum_i (N_i^2-1)Q_i^4}{\sum_i N_i Q_i^4}\,k, \tag{3.2}$$

where

$$k \equiv \frac{\sum_{\{\lambda\}} {\rm Re}\Big[M^{(2)}_{\{\lambda\}} M^{(1)\,*}_{\{\lambda\}}\Big]}{\sum_{\{\lambda\}} |M^{(1)}_{\{\lambda\}}|^2}\,. \tag{3.3}$$

The label i runs over the number of quarks and leptons with masses much less than $\sqrt{s}$; $N_i = 3$ for quarks, $N_i = 1$ for leptons; and Q_i is the fermion charge. For energies between m_b and m_W, for example, $(\sum_i (N_i^2-1)Q_i^4)/(\sum_i N_i Q_i^4) = 70/87$. For energies above m_W, one should add the W loop contributions to $\mathcal{M}^{\rm 1-loop}_{\{\lambda\}}$. This dilutes the QCD corrections considerably, since the W loops quickly dominate [4, 5] (see fig. 1), and they have no QCD corrections.

In fig. 3, k is plotted as a function of the center-of-mass scattering angle θ. Due to Bose symmetry, only the forward region $\cos\theta > 0$ has to be plotted. We also plot the corresponding curves for fully circularly polarized initial photons, but summing over final-state helicities,

$$k_{\lambda_1\lambda_2} \equiv \frac{\sum_{\lambda_3,\lambda_4} {\rm Re}\Big[M^{(2)}_{\{\lambda\}} M^{(1)\,*}_{\{\lambda\}}\Big]}{\sum_{\lambda_3,\lambda_4} |M^{(1)}_{\{\lambda\}}|^2}\,. \tag{3.4}$$

Taking into account CP invariance, there are two independent cases, $++$ and $+-$. Although the QCD corrections are of order α_s/π for these two cases, they have opposite signs, and in the unpolarized cross section there is a large cancellation. The QCD

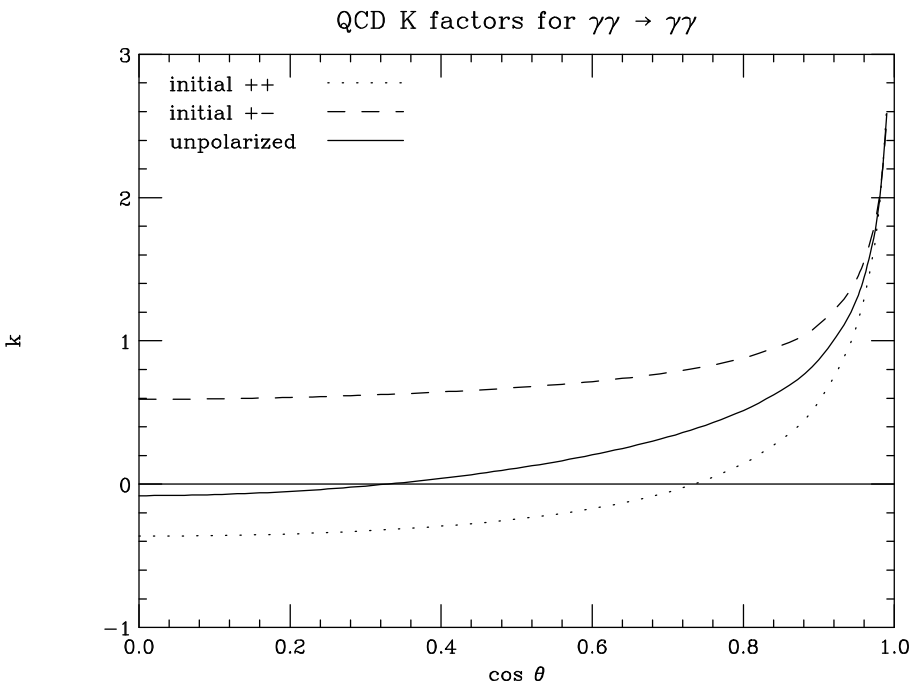

Figure 3: Eqs. (3.2)–(3.4) express the QCD-correction K factor in terms of the quantities k (unpolarized initial and final photons), k_{++} and k_{+-} (fully polarized initial photons). Here k (solid), k_{++} (dotted) and k_{+-} (dashed) are plotted as a function of $\cos\theta$.

corrections to the unpolarized cross section are only of order $0.1 \times \alpha_s/\pi$ for central scattering angles, becoming as large as α_s/π only for $|\cos\theta| \geq 0.95$.

Figure 4 displays the QCD corrections to the cross section in the 10–100 GeV region where quark boxes are important, and the quarks can be taken to be approximately massless. The QED corrections can be neglected in this region as they are a factor of 8 or so smaller. The two independent initial helicity configurations are shown, after integrating the differential cross section with an acceptance cut of $30^\circ < \theta < 150^\circ$, and multiplying by s as in fig. 1. The QCD corrections were computed by multiplying the leading order one-loop result, which contains the full fermion (and W) mass dependence, by the K factor formula (3.2) evaluated for massless fermions in both numerator and denominator (which are of course integrated separately over θ). We can apply eq. (3.2) even across the b quark threshold, simply because the b quark's small charge of $-1/3$ lends it a tiny contribution to the $\gamma\gamma \to \gamma\gamma$ cross section. (Nevertheless, we interpolate $(\sum_i (N_i^2 - 1)Q_i^4)/(\sum_i N_i Q_i^4)$ from $272/345 \approx 0.788$ to $70/87 \approx 0.805$ across the threshold.) We see that the QCD corrections are numerically rather small for central scattering angles in this entire energy range. The small size of the correction explicitly demonstrates the reliability of the leading order prediction.

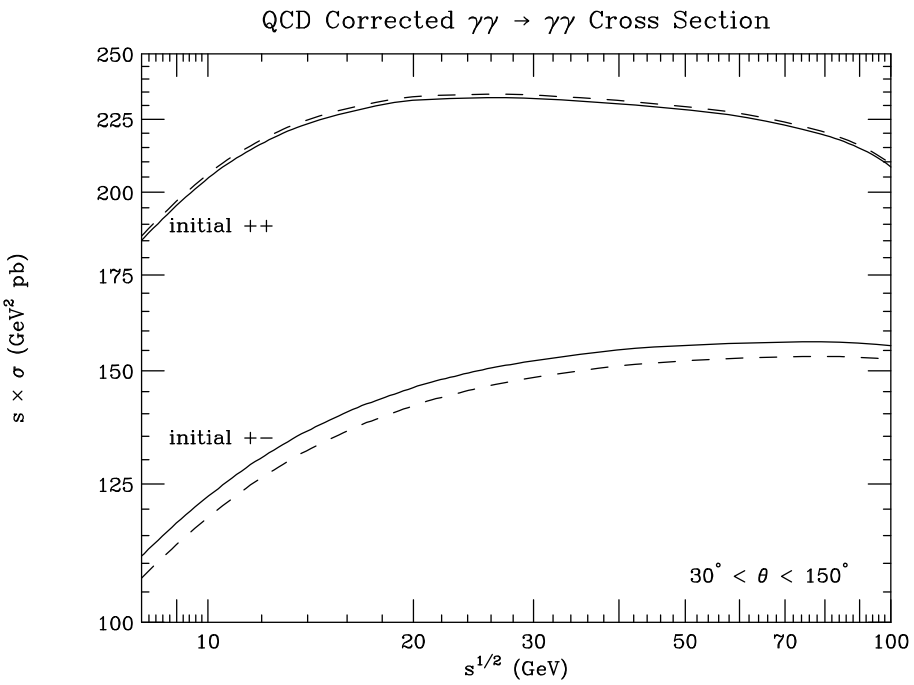

Figure 4: QCD corrections to $\gamma\gamma \to \gamma\gamma$ in the intermediate energy region 8 GeV $< \sqrt{s} <$ 100 GeV where quark boxes are important, for $\alpha_s(m_Z) = 0.118$, and renormalization scale $\mu = \sqrt{s}$. Plotted are the results at leading order (dashed), and including the QCD corrections (solid), for the same quark masses used in fig. 1.

The QED corrections can also be extracted from fig. 3. In the region between m_e and m_μ, for example, the corrections to the unpolarized cross section are

$$\frac{d\sigma^{\rm QED}}{d\cos\theta} = \frac{d\sigma^{\rm LO}}{d\cos\theta} \times \left[1 + 2\frac{\alpha(\mu)}{\pi}\, k\right]. \tag{3.5}$$

For the same angular cuts ($30^\circ < \theta < 150^\circ$) as in the QCD case, this amounts to only a 0.07% decrease in the cross section for ++ initial helicities, and a 0.35% increase for +− initial helicities. It will be a true challenge to measure the $\gamma\gamma \to \gamma\gamma$ reaction to this level of precision.

4. Conclusions

In this paper we presented the two-loop QCD and QED corrections to light-by-light scattering by fermion loops in the ultrarelativistic limit where all kinematic invariants are much greater than the relevant fermion masses. These corrections reliably give the leading Standard Model corrections for most energies below 100 GeV. The corrections are quite small numerically, showing that the leading order computations are robust.

Some of the helicity amplitudes remain quite simple even at two loops, as a consequence of unitarity and a supersymmetry Ward identity for tree amplitudes.

To extend our results to regions where the kinematic invariants are comparable to the masses in the loops, the technology for computing two-loop double box integrals should first be extended to include massive internal lines, which seems feasible. Probably the most important application would then be to compute the electroweak corrections to the W box contribution to $\gamma\gamma \to \gamma\gamma$, since that contribution dominates at high energies, where new physics contributions are most likely to be found.

Acknowledgments

We thank Hooman Davoudiasl and George Gounaris for useful conversations.

A. Two-loop helicity Amplitudes

The explicit expressions for the two-loop amplitudes appearing in eq. (2.6) are

$$M^{(2)}_{--++} = -\frac{3}{2}\,, \tag{A.1}$$

$$M^{(2)}_{-+++} = \frac{1}{8}\Big[\frac{x^2+1}{y^2}((X+i\pi)^2+\pi^2) + \frac{1}{2}(x^2+y^2)((X-Y)^2+\pi^2) - 4\Big(\frac{1}{y}-x\Big)(X+i\pi)\Big] + \Big\{t \leftrightarrow u\Big\}\,, \tag{A.2}$$

$$\begin{aligned} M^{(2)}_{++++} = {} & -2x^2\Big[\mathrm{Li}_4(-x)+\mathrm{Li}_4(-y) - (X+i\pi)\Big(\mathrm{Li}_3(-x)+\mathrm{Li}_3(-y)\Big) \\ & + \frac{1}{12}X^4 - \frac{1}{3}X^3Y + \frac{\pi^2}{12}XY - \frac{4}{90}\pi^4 + i\frac{\pi}{6}X\Big(X^2-3XY+\pi^2\Big)\Big] \\ & - (x-y)\Big(\mathrm{Li}_4(-x/y) - \frac{\pi^2}{6}\mathrm{Li}_2(-x)\Big) \\ & - x\Big[2\mathrm{Li}_3(-x) - \mathrm{Li}_3(-x/y) - 3\zeta_3 - 2(X+i\pi)\mathrm{Li}_2(-x) \\ & \quad + (X-Y)(\mathrm{Li}_2(-x/y)+X^2) + \frac{1}{12}(5(X-Y)+18i\pi)((X-Y)^2+\pi^2) \\ & \quad - \frac{2}{3}X(X^2+\pi^2) - i\pi(Y^2+\pi^2)\Big] \\ & + \frac{1}{4}\frac{1-2x^2}{y^2}((X+i\pi)^2+\pi^2) - \frac{1}{8}(2xy+3)((X-Y)^2+\pi^2) + \frac{\pi^2}{12} \\ & + \Big(\frac{1}{2y}+x\Big)(X+i\pi) - \frac{1}{4} + \Big\{t \leftrightarrow u\Big\}\,, \end{aligned} \tag{A.3}$$

$$
\begin{aligned}
M^{(2)}_{+--+} = -2\frac{x^2+1}{y^2}\Big[&\mathrm{Li}_4(-x/y) - \mathrm{Li}_4(-y) + \frac{1}{2}(X - 2Y - i\pi)(\mathrm{Li}_3(-x) - \zeta_3) \\
&+\frac{1}{24}(X^4 + 2i\pi X^3 - 4XY^3 + Y^4 + 2\pi^2 Y^2) + \frac{7}{360}\pi^4\Big] \\
- 2\frac{x-1}{y}\Big[&\mathrm{Li}_4(-x) - \zeta_4 - \frac{1}{2}(X + i\pi)(\mathrm{Li}_3(-x) - \zeta_3) \\
&+\frac{\pi^2}{6}\Big(\mathrm{Li}_2(-x) - \frac{\pi^2}{6} - \frac{1}{2}X^2\Big) - \frac{1}{48}X^4\Big] \\
+ \Big(2\frac{x}{y} - 1\Big)\Big[&\mathrm{Li}_3(-x) - (X + i\pi)\mathrm{Li}_2(-x) + \zeta_3 - \frac{1}{6}X^3 - \frac{\pi^2}{3}(X + Y)\Big] \\
+ 2\Big(2\frac{x}{y} + 1\Big)\Big[&\mathrm{Li}_3(-y) + (Y + i\pi)\mathrm{Li}_2(-x) - \zeta_3 + \frac{1}{4}X(2Y^2 + \pi^2) \\
&-\frac{1}{8}X^2(X + 3i\pi)\Big] - \frac{1}{4}(2x^2 - y^2)((X - Y)^2 + \pi^2) \\
- \frac{1}{4}\Big(3 + 2\frac{x}{y^2}\Big)&((X + i\pi)^2 + \pi^2) - \frac{2 - y^2}{4x^2}((Y + i\pi)^2 + \pi^2) + \frac{\pi^2}{6} \\
+ \frac{1}{2}(2x + y^2)\Big[&\frac{1}{y}(X + i\pi) + \frac{1}{x}(Y + i\pi)\Big] - \frac{1}{2}\,. \qquad \text{(A.4)}
\end{aligned}
$$

Here

$$
x \equiv \frac{t}{s}\,, \quad y \equiv \frac{u}{s}\,, \quad X \equiv \ln\Big(-\frac{t}{s}\Big)\,, \quad Y \equiv \ln\Big(-\frac{u}{s}\Big)\,. \qquad \text{(A.5)}
$$

References

[1] H. Euler and B. Kochel, Naturwissenschaften, **23**, 246 (1935);
H. Euler and W. Heisenberg, Z. Phys. **98**, 718 (1936);
J. Schwinger, Phys. Rev. **82**, 664 (1951).

[2] R. Karplus and M. Neuman, Phys. Rev. **83**, 776 (1951).

[3] A.I. Akhiezer, Physik. Z. Sowjetunion **11**, 263 (1937).

[4] G. Jikia and A. Tkabladze, Phys. Lett. B **323**, 453 (1994) [hep-ph/9312228].

[5] G.J. Gounaris, P.I. Porfyriadis and F.M. Renard, Phys. Lett. B **452**, 76 (1999) [hep-ph/9812378].

[6] S.A. Lee *et al.*, *Measurement of the magnetically-induced QED birefringence of the vacuum and an improved laboratory search for light pseudoscalars*, FERMILAB-PROPOSAL-P-877A;
D. Bakalov, *An overview of the nonlinear QED effects in the context of measurements of vacuum birefringence in the PVLAS experiment: Early estimates*, preprint INFN-AE-94-27;

G. Cantatore *et al.*, *Experimental study of the quantum vacuum. Production and detection of dark matter candidates in the PVLAS experiment*, in *Dark matter: proceedings of DM97, 1st Italian conference on dark matter*, Trieste (Studio Editoriale Fiorentino, 1998).

[7] G. Godfrey, private communication.

[8] H. Cheng and T.T. Wu, Phys. Rev. **182**, 1873 (1969); Phys. Rev. D **2**, 2444 (1970); Phys. Rev. D **5** (1972) 3077;
A.I. Milstein and M. Schumacher, Phys. Rept. **243**, 184 (1994);
Sh. Zh. Akhmadaliev, et al., Phys. Rev. **C58**, 2844 (1998) [hep-ex/9806037].

[9] R.S. Van Dyck, P.B. Schwinberg and H.G. Dehmelt, Phys. Rev. Lett. **59**, 26 (1987).

[10] H.N. Brown *et al.* [Muon $g-2$ Collaboration], Phys. Rev. Lett. **86**, 2227 (2001) [hep-ex/0102017].

[11] I.F. Ginzburg, G.L. Kotkin, V.G. Serbo and V.I. Telnov, JETP Lett. **34**, 491 (1981) [Pisma Zh. Eksp. Teor. Fiz. **34**, 514 (1981)].

[12] K. Cheung, Phys. Rev. D **61**, 015005 (2000) [hep-ph/9904266];
H. Davoudiasl, Phys. Rev. D **60**, 084022 (1999) [hep-ph/9904425]; Int. J. Mod. Phys. A **15**, 2613 (2000) [hep-ph/0001248].

[13] N. Arkani-Hamed, S. Dimopoulos and G. Dvali, Phys. Lett. B **429**, 263 (1998) [hep-ph/9803315];
I. Antoniadis, N. Arkani-Hamed, S. Dimopoulos and G. Dvali, Phys. Lett. B **436**, 257 (1998) [hep-ph/9804398].

[14] V.I. Ritus, Sov. Phys. JETP **42**, 774 (1975) [Pisma Zh. Eksp. Teor. Fiz. **69**, 1517 (1975)];
W. Dittrich and M. Reuter, *Effective Lagrangians in Quantum Electrodynamics*, Lect. Notes Phys. **220**, 1 (Springer, 1985);
M. Reuter, M.G. Schmidt and C. Schubert, Annals Phys. **259**, 313 (1997) [hep-th/9610191];
D. Fliegner, M. Reuter, M.G. Schmidt and C. Schubert, Theor. Math. Phys. **113**, 1442 (1997) [hep-th/9704194];
C. Schubert, hep-th/0101036, to appear in Phys. Rept.

[15] E.W. Glover, C. Oleari and M.E. Tejeda-Yeomans, Nucl. Phys. B **605**, 467 (2001).

[16] W.L. van Neerven, Nucl. Phys. **B268**, 453 (1986);
Z. Bern, L. Dixon, D.C. Dunbar and D.A. Kosower, Nucl. Phys. **B425**, 217 (1994) [hep-ph/9403226];
Z. Bern, L. Dixon and D.A. Kosower, Ann. Rev. Nucl. Part. Sci. **46**, 109 (1996) [hep-ph/9602280].

[17] Z. Bern, J.S. Rozowsky and B. Yan, Phys. Lett. **B401**, 273 (1997) [hep-ph/9702424].

[18] Z. Bern, L. Dixon and D.A. Kosower, JHEP **0001**, 027 (2000) [hep-ph/0001001].

[19] V.A. Smirnov, Phys. Lett. **B460**, 397 (1999) [hep-ph/9905323];
V.A. Smirnov and O.L. Veretin, Nucl. Phys. **B566**, 469 (2000) [hep-ph/9907385].

[20] C. Anastasiou, E.W.N. Glover and C. Oleari, Nucl. Phys. **B565**, 445 (2000) [hep-ph/9907523];
C. Anastasiou, E.W.N. Glover and C. Oleari, Nucl. Phys. **B575**, 416 (2000), err. ibid. **B585**, 763 (2000) [hep-ph/9912251].

[21] T. Gehrmann and E. Remiddi, Nucl. Phys. Proc. Suppl. **89**, 251 (2000) [hep-ph/0005232];
C. Anastasiou, J.B. Tausk and M.E. Tejeda-Yeomans, Nucl. Phys. Proc. Suppl. **89**, 262 (2000) [hep-ph/0005328].

[22] M.T. Grisaru, H.N. Pendleton and P. van Nieuwenhuizen, Phys. Rev. D **15**, 996 (1977);
M.T. Grisaru and H.N. Pendleton, Nucl. Phys. B **124**, 81 (1977);
S.J. Parke and T.R. Taylor, Phys. Lett. B **157**, 81 (1985), err. ibid. **174B**, 465 (1985).

[23] W.H. Furry, Phys. Rev. **51**, 125 (1937).

[24] Z. Bern, A. DeFreitas, L. Dixon and H.L. Wong, to appear.

[25] Z. Bern, A. De Freitas, L. Dixon, and A. Ghinculov, in preparation.

[26] See e.g. K.S. Kölbig, SIAM J. Math. Anal. **17**, 1232 (1986).

[27] K.S. Kölbig, J.A. Mignaco and E. Remiddi, B.I.T. **10**, 38 (1970).

[28] L. Lewin, *Dilogarithms and Associated Functions* (Macdonald, 1958).

[29] G.J. Gounaris, P.I. Porfyriadis and F.M. Renard, Eur. Phys. J. C **9**, 673 (1999) [hep-ph/9902230].

[30] E.W. Glover and J.J. van der Bij, Nucl. Phys. B **321**, 561 (1989).

[31] Z. Bern, A. De Freitas and L. Dixon, preprint hep-ph/0109078.

[32] Z. Bern, L. Dixon and C. Schmidt, in preparation.

[33] H. Cheng and T.T. Wu, Phys. Rev. **182**, 1852 (1969); Phys. Rev. D **1**, 3414 (1970).